Bull. Mater. Sci., Vol. 23, No. 5, October 2000, pp. 383–391. © Indian Academy of Sciences.

Kinetics of hydrogen evolution reaction on $Zr_{0·5}Ti_{0·5}V_{0·6}Cr_{0·2}Ni_{1·2}$ alloy in KOH electrolyte

SHALINI RODRIGUES, N MUNICHANDRAIAH[†]* and A K SHUKLA*

Solid State and Structural Chemistry Unit, [†]Department of Inorganic and Physical Chemistry, Indian Institute of Science, Bangalore 560 012, India

MS received 10 August 2000

Abstract. A hydrogen-storage alloy of the composition $Zr_{0·5}Ti_{0·5}V_{0·6}Cr_{0·2}Ni_{1·2}$ has been investigated for corrosion resistance and hydrogen-evolution reaction (HER) in KOH electrolyte of varying concentrations. Activation of the electrode by absorption of hydrogen takes place after prolonged cathodic polarization in the potential range of HER. Prior to activation, the open-circuit potential is about – 0·4 V vs Hg/HgO, OH^-, at which the alloy electrode tends to undergo corrosion with oxygen-reduction reaction (ORR) as the conjugate reaction. The corrosion–current density measured from Tafel polarization of ORR is found to be independent of KOH concentration and has an average value of about 30 μA cm^{-2}. Subsequent to activation, the open circuit potential of the electrode is shifted to about – 0·93 V vs Hg/HgO, OH^-, which is equal to the reversible potential of HER. The exchange current density values measured from Tafel polarization of HER are marginally higher in relation to the values obtained before the electrode is activated. Alternating-current impedance spectra in the Nyquist form contain two overlapped semicircles. The high-frequency semicircle is attributed to the electrode geometry, while the low-frequency semicircle is due to the charge-transfer reaction and double–layer capacitance. The impedance data are analyzed by a non-linear least square curve fitting technique and impedance parameters are evaluated.

Keywords. Hydrogen-storage alloy; hydrogen-evolution reaction; Tafel polarization; a.c. impedance; exchange-current density.

1. Introduction

In recent years, replacement of the toxic cadmium electrodes of nickel/cadmium batteries with metal hydride (MH) electrodes has resulted in environment friendly nickel/metal hydride (Ni/MH) batteries. However, the development of metal hydride (MH) electrode materials, which yield high energy per unit weight with a long charge/discharge cycle life, has been challenging. To this end, several AB_2 and AB_5-type alloys have been investigated (Appleby *et al* 1973). Although AB_5-type alloys were preferred in the past, presently the preference is for AB_2-type alloys (Ganesh Kumar 1999). When a metal hydride electrode in an alkaline electrolyte (usually 6 M KOH) is subjected to charging, reduction of H_2O molecule takes place producing atomic hydrogen on its surface in adsorbed state. Penetration of adsorbed hydrogen into the bulk of the electrode material results in the formation of metal hydride, which behaves as a reservoir of hydrogen in the rechargeable battery. Accordingly, the formation of metal hydride is an intermediate step of hydrogen-evolution reaction (HER) on hydrogen adsorbing alloys, which has been a subject of extensive investigation at various electrode materials both in acidic and alkaline electrolytes (Frumkin 1963; Enyo 1983; Trasatti 1992).

An AB_2-type hydrogen adsorbing alloy of the composition $Zr_{0·5}Ti_{0·5}V_{0·6}Cr_{0·2}Ni_{1·2}$ was recently investigated for rechargeable Ni/MH and Ag/MH batteries (Ganesh Kumar *et al* 1998, 1999, 2000; Rodrigues *et al* 1999a). The MH electrodes were made by pasting fine particles of this alloy mixed with PTFE binder on Ni-current collectors. An electrode required several (~ 10) charge/discharge cycles of activation in 6 M KOH to achieve a maximum discharge capacity of ~ 320 mAh g^{-1}. During the process of activation, the alloy surface apparently became conducive for penetration of absorbed hydrogen atoms inside the particles. Subsequent to activation, the open-circuit potential (OCP) of the MH electrode reached a value close to the reversible potential of HER, viz. – 0·93 V vs Hg/HgO, OH^-, from a state of mixed potential. Thus, the HER appears to be sensitive to the catalytic and adsorptive nature of the electrode surface. The surface nature of the alloy before activation could be different from the surface nature after hydride formation. Accordingly, the kinetics of HER are expected to differ before and after hydride formation. In this communication, we therefore report the kinetics of HER studies by d.c. polarization and

*Authors for correspondence

a.c. impedance spectroscopy on a $Zr_{0.5}Ti_{0.5}V_{0.6}Cr_{0.2}Ni_{1.2}$ alloy ingot electrode before and after its activation. The study suggests that the alloy ingot has a tendency to corrode prior to its activation but corrosion reaction is seemingly ceased subsequent to the hydride formation.

2. Experimental

An ingot of about 500 g of $Zr_{0.5}Ti_{0.5}V_{0.6}Cr_{0.2}Ni_{1.2}$ alloy was prepared from the spongy elements by repeated arc melting in an argon atmosphere. A powdered sample of the ingot was subjected to XRD and SEM studies. The data suggested that the alloy was homogeneous in composition and its structure conformed to AB_2-Laves phase. Small pieces of the alloy were separated from the ingot and surfaces of these pieces were polished to a smooth finish. An electrode was made by mounting an ingot in a PTFE holder, which was provided with a stainless steel current collecting rod. The crevices between the ingot electrode and PTFE were sealed with an epoxy resin. Area of the electrodes exposed to the electrolyte was in the range of 0·16–0·2 cm^2. The electrodes were etched in concentrated HCl for a few seconds, washed copiously in distilled water and dried at 80°C before use. The electrode was inserted into a glass cell, which was fitted with two symmetrical large area nickel counter electrodes and a Hg/HgO, OH^- (6 M KOH) reference electrode (MMO). Experiments were carried out in KOH electrolyte of varying concentrations in the range between 0·2 M and 6 M which were prepared using analar grade KOH in doubly-distilled water and were subjected to pre-electrolysis before use.

Polarization experiments were carried out in stirred electrolytes by sweeping the electrode potential at a scan rate of 0·1 mV s^{-1} employing a potentiostat (EG&G PARC Versastat). Cyclic voltammetric experiments were carried out in unstirred electrolytes at a scan rate of 10 mV s^{-1}. A.c. impedance spectroscopy was carried out in the frequency range 100 kHz–10 mHz at an excitation signal of 5 mV using electrochemical impedance analyzer (EG&G PARC model 6310). The impedance data were analyzed by non-linear least square fitting procedure (Boukamp 1989). All experiments were carried out at 20 ± 1°C.

3. Results and discussion

A $Zr_{0.5}Ti_{0.5}V_{0.6}Cr_{0.2}Ni_{1.2}$ alloy electrode was subjected to potential cycling in 6 M KOH covering both the HER and oxygen-evolution reaction (OER) (figure 1). The increase in current at about – 1·2 V vs MMO is due to HER. It is noteworthy that the HER is shifted cathodically by about 0·3 V from its reversible value of – 0·93 V vs MMO. In a similar fashion, the OER occurs at potentials positive to 0·6 V vs MMO, which is also shifted anodically from its reversible value of 0·3 V vs MMO. In the potential region close to the commencement of OER, a pair of current peaks appears which could be attributed to oxidation of one of the metallic constituents of the $Zr_{0.5}Ti_{0.5}V_{0.6}Cr_{0.2}Ni_{1.2}$ alloy electrode. Considering the composition of the alloy, the metallic element undergoing oxidation appears to be Ni.

The OCP of the alloy electrode in KOH electrolyte was in the range between – 0·2 and – 0·4 V vs MMO. Subsequent to its activation, however, it equilibrated to about –0·93 V vs MMO, which is the reversible potential for HER. This suggests that the electrode behaves as a reversible hydrogen electrode only after its activation. Prior to this, it is under a state of corrosion and the open-circuit potential ($E_{cor} \approx -0{\cdot}4$ V vs MMO) is a mixed potential. The partial reactions, which impart a mixed potential to the electrode, could schematically be written as follows:

$$M \rightarrow M^n + ne^-, \qquad (1)$$

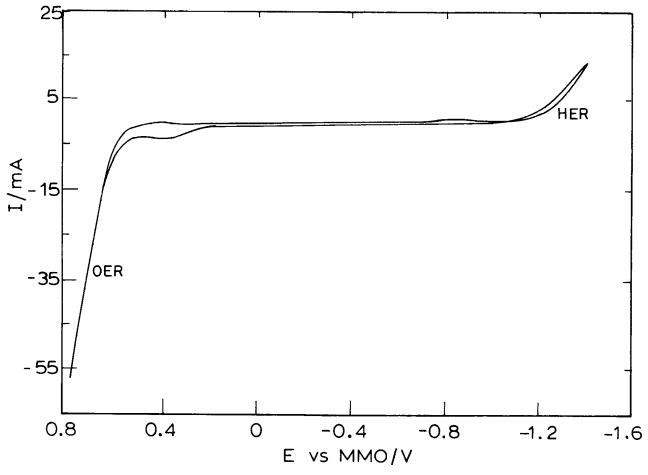

Figure 1. Cyclic voltammogram of a $Zr_{0.5}Ti_{0.5}V_{0.6}Cr_{0.2}Ni_{1.2}$ alloy electrode in 6 M KOH in the potential range between – 1·4 V and + 0·8 V vs MMO at a scan rate of 10 mV s^{-1}. Area of the electrode: 0·16 cm^2.

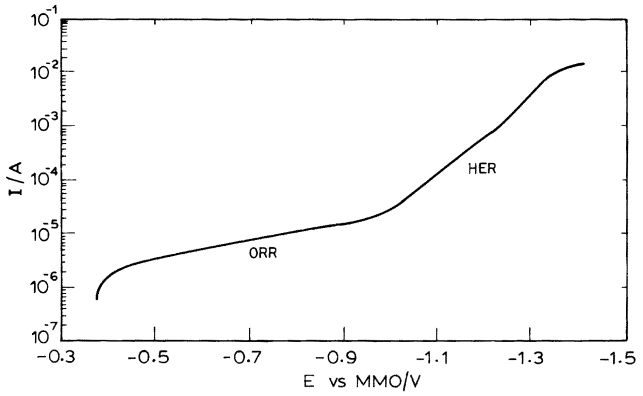

Figure 2. Tafel plot of a $Zr_{0.5}Ti_{0.5}V_{0.6}Cr_{0.2}Ni_{1.2}$ alloy electrode in 6 M KOH in the potential range between – 0·35 V and – 1·4 V vs MMO. Area of the electrode: 0·16 cm^2.

Table 1. Electrode kinetic data for the corrosion (i_{cor}) and HER (Tafel slope, a and i_0) occurring on the $Zr_{0·5}Ti_{0·5}V_{0·6}Cr_{0·2}Ni_{1·2}$ electrode prior to its activation in KOH electrolyte.

C_{KOH} (M)	0·2	0·4	0·6	0·8	1·0	2·0	3·0	4·0	5·0	6·0
Tafel slope (V)	0·168	0·159	0·156	0·146	0·167	0·167	0·130	0·146	0·146	0·146
a	0·357	0·377	0·384	0·410	0·370	0·359	0·461	0·410	0·410	0·400
$i_0 \times 10^5$ (A cm^{-2})	5·63	3·13	2·50	1·88	3·75	1·25	1·88	4·38	2·50	6·25
$i_{cor} \times 10^5$ (A cm^{-2})	1·06	1·25	2·5	1·88	1·25	1·25	1·25	1·25	3·75	3·0

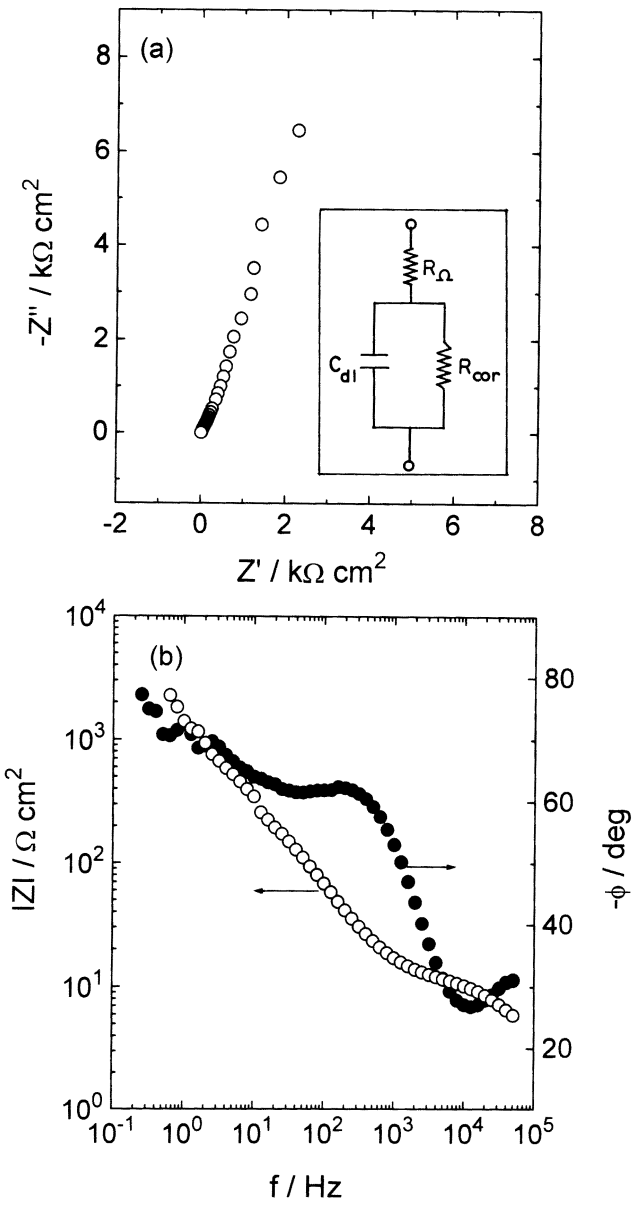

Figure 3. A.c. impedance spectrum in (**a**) Nyquist, and (**b**) Bode forms of a $Zr_{0·5}Ti_{0·5}V_{0·6}Cr_{0·2}Ni_{1·2}$ alloy electrode in 6 M KOH. The equivalent circuit is shown as the inset. The symbols: Z', Z'', $|Z|$, f, R_Ω, R_{cor} and C_{dl} refer to real component of impedance, imaginary component of impedance, modulus of impedance, phase angle, ohmic resistance, corrosion resistance and double-layer capacitance, respectively.

$$O + ne^- \rightarrow R. \quad (2)$$

Reaction (1) represents the oxidation of metal (M) or a metallic element of the alloy, which undergoes corrosion and reaction (2) represents the conjugate reaction in which the electrons liberated during reaction (1) are consumed. The corrosion potential (E_{cor}) is determined by the kinetics of both these reactions. In the present case, since the corrosion potential of the alloy ingot is positive to the reversible potential for HER by about 0·5 V, HER cannot take place as the cathodic conjugate reaction. Consequently, the reduction of dissolved oxygen in the electrolyte (ORR),

$$O_2 + 2H_2O + 4e^- \rightarrow 4OH^-, \quad (3)$$

is the most probable reaction.

The cathodic polarization behaviour of the electrode is shown in figure 2. Two linear segments of the cathodic polarization curve are clearly present in KOH electrolyte with varying concentrations employed during this study. The segment between E_{cor} and – 0·93 V vs MMO is the Tafel component of ORR (reaction 3) and the other segment at potentials cathodic to – 0·93 V vs MMO is due to HER. The value of corrosion current density (i_{cor}) obtained by extrapolation of the ORR Tafel line to E_{cor} is 30 µA cm^{-2}.

In order to substantiate reaction (3) as the cathodic conjugate reaction during corrosion of the alloy ingot, polarization experiments were also conducted in O_2 saturated and de-aerated (by argon gas) 6 M KOH electrolyte. The values of i_{cor} obtained are 130 µA cm^{-2} and 6 µA cm^{-2} in O_2 saturated and de-aerated 6 M KOH electrolyte, respectively. An increase in the value of i_{cor} in O_2 saturated electrolyte and a decrease in the de-aerated electrolyte clearly suggests reaction (3) to be the cathodic reaction for corrosion of the alloy ingot. Polarization measurements were carried out in aerated KOH electrolytes of varying concentrations and i_{cor} values were obtained as given in table 1. Interestingly little dependence of i_{cor} of the alloy was observed on KOH concentration.

A.c. impedance data of the alloy ingot at OCP are shown in figure 3 as Nyquist and Bode plots. The appropriate equivalent circuit comprising corrosion resistance (R_{cor}) of the alloy, double-layer capacitance (C_{dl}) and

electrolyte resistance (R_{Ω}) is shown as the inset. The impedance data do not take the shape of a semicircle in the Nyquist plot (figure 3a), suggesting a high value of R_{cor}. The Bode plot (figure 3b) also suggests capacitive behaviour of the electrode as logarithmic modulus of impedance ($\log |Z|$) varies linearly with logarithmic frequency ($\log f$) with a slope of – 0·8, which is close to the theoretical value of – 1 for a pure capacitor. Also, the phase angle (f) is about – 70° over a wide frequency range. Under these conditions, $|Z|$ is related to C_{dl}, as follows:

$$\log |Z| = -\log w - \log C_{dl}, \tag{4}$$

where $w = 2pf$. When $w = 1$, $\log |Z|$ becomes equal to $-\log C_{dl}$. The value of C_{dl} obtained from figure 3b is 0·3 mF cm^{-2}. This value of C_{dl} for $Zr_{0·5}Ti_{0·5}V_{0·6}Cr_{0·2}Ni_{1·2}$ electrode is much higher than the C_{dl} (about 20 μF cm^{-2}) for Hg/solution interface. Similar to the present study, high values of C_{dl} are reported for solid electrodes such as Ni, Ni–Zn alloy, etc in alkaline electrolytes (Chen and Lasia 1991; Dumont *et al* 1993). The high values of C_{dl} are perhaps due to pseudo capacitance, which arises due to adsorption of O_2, OH^- or intermediates of reaction (1) at the alloy electrode/electrolyte interface. From impedance spectra recorded at different potentials, C_{dl} values were evaluated. The variation of C_{dl} with the electrode potential is shown in figure 4. The increase of C_{dl} with increase of negative potential of the electrode could also be due to adsorption of intermediates of ORR (reaction 3), which occurs in the potential range between – 0·2 and – 0·6 V vs MMO.

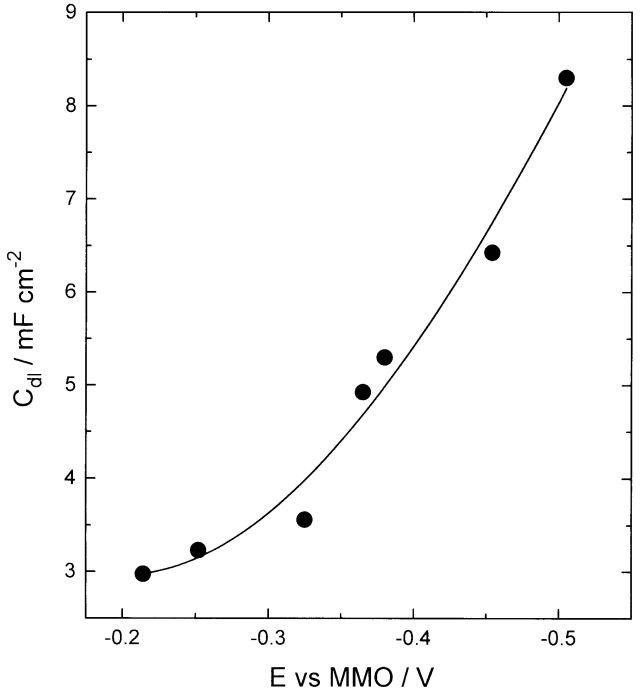

Figure 4. Variation of double-layer capacitance (C_{dl}) as a function of electrode potential (E) of the alloy prior to its activation.

The second region of the polarization curve (figure 2) is due to HER:

$$2H_2O + 2e^- \rightarrow H_2 + 2OH^-. \tag{5}$$

The mechanism of HER is generally considered to comprise the following three steps (Chen and Lasia 1991; Spataru *et al* 1996; Notoya 1997):

$$H_2O + M + e^- \underset{k_{-1}}{\overset{k_1}{\rightleftharpoons}} MH_s + OH^-, \tag{6}$$

$$MH_s + H_2O + e^- \underset{k_{-2}}{\overset{k_2}{\rightleftharpoons}} H_2 + M + OH^-, \tag{7}$$

$$2MH_s \underset{k_{-3}}{\overset{k_3}{\rightleftharpoons}} H_2 + 2M. \tag{8}$$

The first step (reaction 6), known as Volmer reaction, is the primary electron transfer step resulting in the formation of hydrogen adsorbed on the electrode surface (MH_s) from H_2O molecule. It is followed by the second step (reaction 7) or/and the third step (reaction 8) for completion of HER (reaction 5). The reaction (7), known as Heyrovsky reaction, suggests the formation of H_2 molecule by desorption of surface hydrogen and a simultaneous reduction of H_2O molecule. Reaction (8), called as Tafel reaction, suggests the formation of H_2 molecule by a combination of two neighbouring surface hydrogen atoms.

A study of literature reveals that HER on Ni metal and Ni containing alloys proceeds via the Volmer–Heyrovsky mechanism with the Volmer reaction as the rate determining step (rds) (Chen and Lasia 1991; Spataru *et al* 1996; Notoya 1997). In the present study, the alloy electrode consists of Ni as the major element, and therefore the following mechanism is assumed to be valid for HER.

$$H_2O + M + e^- \xrightarrow{k_1} MH_s + OH^-, \tag{9}$$

$$MH_s + H_2O + e^- \underset{k_{-2}}{\overset{k_2}{\rightleftharpoons}} H_2 + M + OH^-. \tag{7}$$

Reaction (9) with a single arrow indicates an irreversible rds and it differs from reaction (6) which suggests an equilibrium process of fast reaction. Under the Tafel conditions (i.e. $(E - E^r) \gg RT/F$), the kinetic equation can be rewritten as:

$$i = i_0 \exp[-a\, fh], \tag{10}$$

where i is current density corresponding to overpotential

h ($= E - E^r$), E the electrode potential, E^r the reversible potential of HER, i_0 the exchange-current density and a the energy-transfer coefficient. By extrapolation of HER Tafel line (figure 2) to E^r (– 0·93 V vs MMO), i_0 is evaluated, and from the Tafel slope (b) the value of a is obtained. The values of i_0, b and a obtained for HER in KOH electrolytes of varying concentrations are given in table 1. The values of these parameters are nearly constant in all solutions suggesting a negligible influence of concentration of KOH on the kinetics of HER at $Zr_{0·5}Ti_{0·5}V_{0·6}Cr_{0·2}Ni_{1·2}$ alloy. The value of i_0 is similar in magnitude to the reported values for HER at several electrodes in KOH electrolytes (Chen and Lasia 1991; Spataru *et al* 1996; Notoya 1997). Although the Tafel slope (b) is expected to be ~ 120 mV assuming $a \approx 0·5$, large deviations from this value are reported in the literature (Appleby *et al* 1973). In the present study also, the values of b obtained are higher than 120 mV (table 1). Accordingly, the values of a (table 1) are marginally lesser than 0·5.

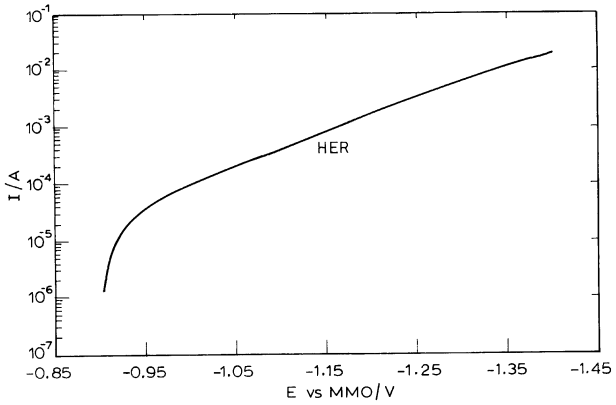

Figure 5. Tafel plot of a $Zr_{0·5}Ti_{0·5}V_{0·6}Cr_{0·2}Ni_{1·2}$ alloy electrode in 6 M KOH in the potential range between – 0·90 V and – 1·4 V vs MMO. Area of the electrode: 0·16 cm^2.

Since the alloy electrode has been proven for its hydrogen absorbing capability as reported previously by studying battery grade laboratory scale electrodes, cells and battery (Ganesh Kumar *et al* 1998, 1999, 2000; Rodrigues *et al* 1999a), it was polarized cathodically at a current density of 2 mA cm^{-2} for absorption of hydrogen, which resulted in vigorous evolution of gas at the electrode surface. During the course of electrolysis, the passage of current was intermittently terminated and open-circuit potential of the electrode was measured. A shift in open-circuit potential from E_{cor} to the theoretical reversible hydrogen evolution reaction potential (– 0·93 V vs MMO) was taken to be the indication for absorption of the atomic hydrogen by the alloy electrode. It was found that considerable length of polarization was required to activate the electrode and to realize a potential value of – 0·93 V vs MMO. Subsequent to its activation, the potential was stable around – 0·93 V vs MMO and it did not return to E_{cor} even after the electrode was left under open-circuit condition for a prolonged time.

For the purpose of kinetic studies of HER, the activated alloy electrode was subjected to Tafel and a.c. impedance measurements in KOH electrolytes with varying concentrations. Although the alloy behaves as a reversible hydrogen electrode, oxidation of hydrogen is not studied. This is due to the reason that the quantity of absorbed hydrogen in the alloy is so small that the electrode becomes deactivated within a few minutes under anodic conditions. Hence, the polarization as well as the a.c. impedance studies, which require large overpotential range and a long duration of the experiments could not be performed. For a battery grade electrode, which requires storage of a larger charge, the alloy was finely powdered

Table 2. Electrode kinetic data for the HER occurring on the $Zr_{0·5}Ti_{0·5}V_{0·6}Cr_{0·2}Ni_{1·2}$ electrode subsequent to its activation in KOH electrolytes.

C_{KOH} (M)	0·2	0·4	0·6	0·8	1·0	2·0	3·0	4·0	5·0	6·0
Tafel slope (V)	0·188	0·172	0·152	0·175	0·153	0·150	0·169	0·155	0·162	0·170
a	0·319	0·348	0·394	0·341	0·392	0·400	0·354	0·385	0·370	0·352
$i_0 \times 10^5$ (A cm^{-2})	8·13	8·75	4·38	12·5	15·6	8·13	32·5	26·25	21·87	12·20

Table 3. Impedance parameters for the $Zr_{0·5}Ti_{0·5}V_{0·6}Cr_{0·2}Ni_{1·2}$ alloy electrode in 6 M KOH subsequent to its activation (see the text for symbols).

E vs MMO (V)	– 0·936	– 0·971	– 1·03	– 1·074	– 1·17	– 1·229	– 1·28
R_Ω (Ω)	1·338 ± 0·026	1·256 ± 0·021	1·433 ± 0·028	1·195 ± 0·025	1·27 ± 0·027	1·31 ± 0·027	1·58 ± 0·032
R_1 (Ω)	1·244 ± 0·293	1·257 ± 0·248	1·462 ± 0·350	2·306 ± 0·392	2·23 ± 0·624	1·49 ± 0·624	0·97 ± 0·569
$Q_1 \times 10^4$ (Ω^{-1})	4·99 ± 3·5	5·67 ± 3·17	4·62 ± 3·00	4·33 ± 1·68	4·63 ± 2·03	2·69 ± 1·77	2·01 ± 1·88
n_1	0·856 ± 0·081	0·847 ± 0·064	0·845 ± 0·075	0·812 ± 0·045	0·81 ± 0·055	0·86 ± 0·085	0·90 ± 0·122
$R_{ct} \times 10^{-2}$ (Ω)	4·69 ± 0·101	3·99 ± 0·053	2·28 ± 0·038	1·49 ± 0·021	4·31 ± 0·085	2·23 ± 0·089	8·67 ± 0·085
$Q_{dl} \times 10^4$ (Ω^{-1})	9·29 ± 0·235	8·79 ± 0·167	8·22 ± 0·263	7·45 ± 0·254	6·39 ± 0·342	5·64 ± 0·559	6·79 ± 0·085
n_2	0·717 ± 0·006	0·716 ± 0·005	0·722 ± 0·008	0·735 ± 0·008	0·76 ± 0·015	0·76 ± 0·024	0·78 ± 0·048

as reported elsewhere (Ganesh Kumar *et al* 1998, 1999, 2000; Rodrigues *et al* 1999a). A typical cathodic Tafel plot of the alloy electrode in 6 M KOH is shown in figure 5. The presence of linearity of the data over about two orders of magnitude of current suggests that reaction (5) occurs under charge-transfer control. Similar data were obtained in KOH electrolytes of varying concentrations. The values of i_0, b and a obtained in KOH electrolytes for HER at $Zr_{0·5}Ti_{0·5}V_{0·6}Cr_{0·2}Ni_{1·2}$ alloy electrode subsequent to its activation are shown in table 2. Akin to the values of the parameters before activation (table 1), the values after activation (table 2) do not show a strong dependence on the concentration of the electrolyte, although there is some scatter in the values. On an average, the Tafel slope remains the same before and after activation. However, the exchange-current density values are marginally only higher after activation of the electrode than before activation.

A.c. impedance spectra of $Zr_{0·5}Ti_{0·5}V_{0·6}Cr_{0·2}Ni_{1·2}$ alloy electrode in 6 M KOH recorded at – 0·93 V vs MMO and at cathodic overpotentials in HER region are shown in figures 6 and 7 in Nyquist and Bode plots, respectively. The data in a Nyquist plot take the shape of a distorted semicircle suggesting the presence of overlapped semicircles. A study of literature on the impedance of HER in alkaline media revealed the presence of two semicircles (Chen and Lasia 1991; Dumont *et al* 1993). The high-frequency small semicircle was not clearly understood and it was attributed to the geometry of the electrodes schematically by a resistance and a capacitance in parallel

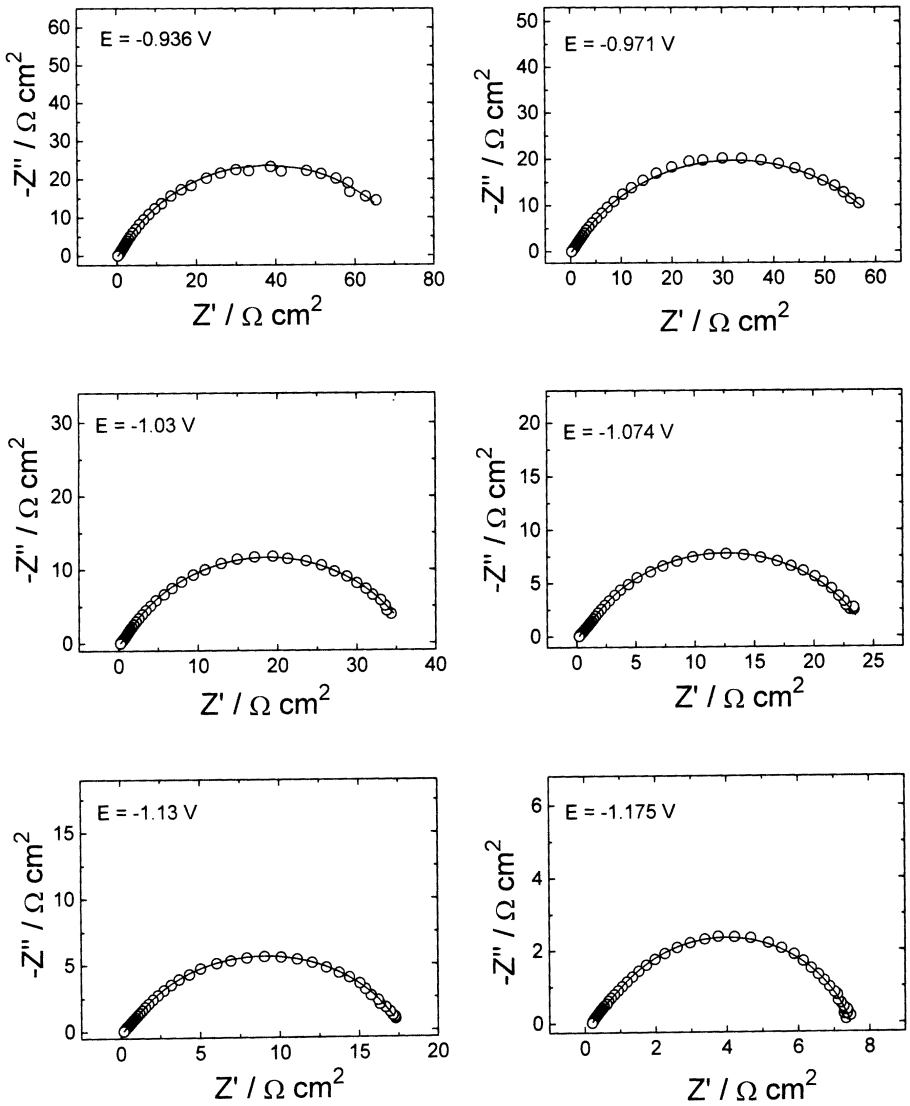

Figure 6. Electrochemical a.c. impedance spectra in Nyquist form of a $Zr_{0·5}Ti_{0·5}V_{0·6}Cr_{0·2}Ni_{1·2}$ alloy electrode in 6 M KOH at different potentials (E vs MMO). The experimental data are shown as symbols and the theoretical data obtained from NLLS fit results are shown as solid curves.

(Chen and Lasia 1991; Dumont *et al* 1993). The low-frequency semicircle was due to a parallel arrangement of charge-transfer resistance (R_{ct}) of HER and double-layer capacitance (C_{dl}). The impedance data of the present study are also considered to consist of two semicircles which overlap due to similarity in magnitude of the respective time constants. Since the two semicircles are distorted, an equivalent circuit (figure 8) consisting of constant phase-elements (CPE) in the place of capacitance is considered similar to the studies reported (Munichandraiah *et al* 1998; Rodrigues *et al* 1999a, b). In the equivalent circuit (figure 8), $R_{Ù}$ represents the solution resistance, R_1 and Q_1 represents resistance and constant phase-element of high frequency small semicircle respectively, R_{ct} and Q_{dl} correspond to charge-transfer resistance of HER and CPE in place of double-layer capacitance (C_{dl}), respectively. The admittance representation of CPE is given by:

$$Y^*(w) = Y_0(jw)^n. \tag{11}$$

For $n = 0$, it represents a resistance with $R = Y_0^{-1}$; for $n = 1$, a capacitance with $C = Y_0$; for $n = 0{\cdot}5$, a Warburg; and for $n = -1$ an inductance with $L = Y_0^{-1}$ (Boukamp 1989).

The impedance data of HER were subjected to NLLS fitting, the impedance parameters obtained are given in table 3 and the theoretical curves are shown as solid lines in figures 6 and 7. The theoretical curves agree well with the experimental data. Charge-transfer resistance (R_{ct}) measured at overpotentials is approximately related to i_0 and a of HER as described below (Elumalai *et al* 1999).

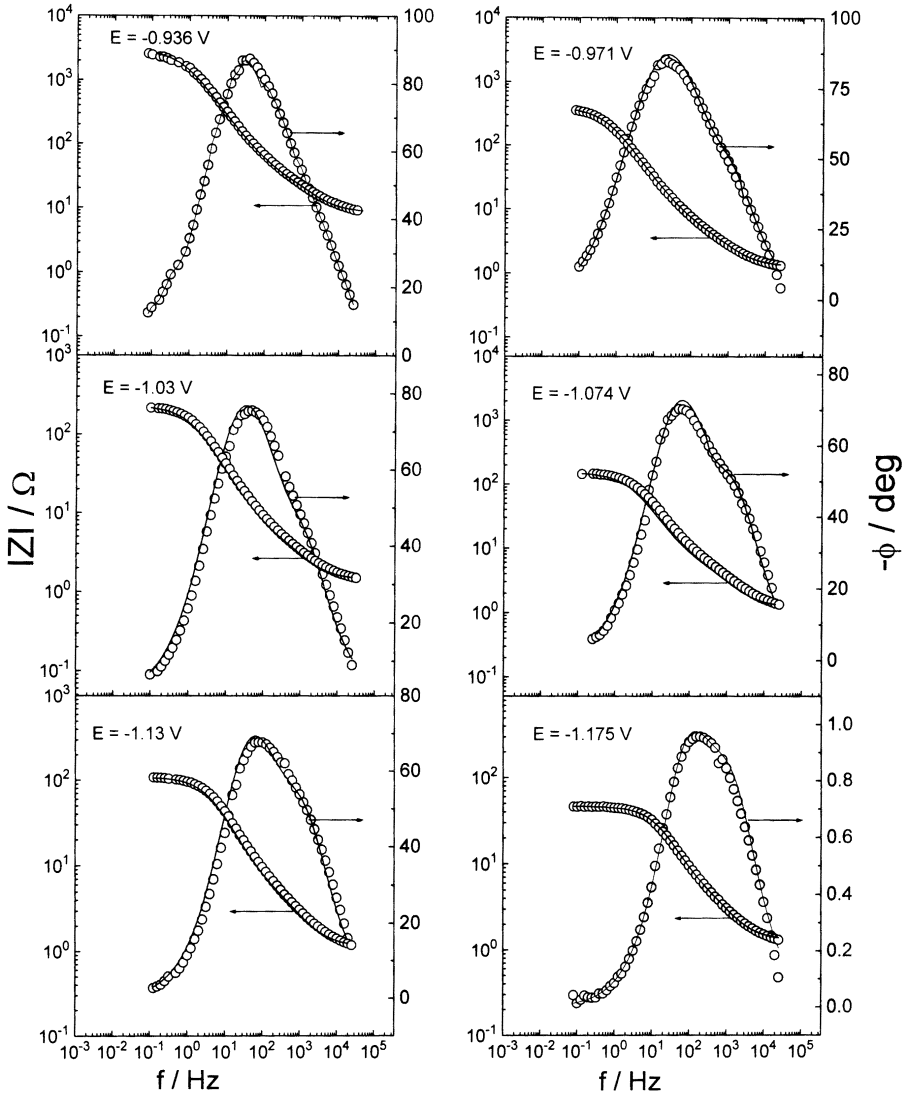

Figure 7. Electrochemical a.c. impedance spectra in Bode form of a $Zr_{0·5}Ti_{0·5}V_{0·6}Cr_{0·2}Ni_{1·2}$ alloy electrode in 6 M KOH at different potentials (E vs MMO). The experimental data are shown as symbols and the theoretical data obtained from NLLS fit results are shown as solid curves.

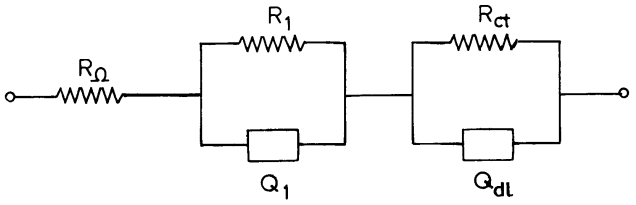

Figure 8. Equivalent circuit used for NLLS fit. R_Ω, R_1 and R_2 refer to ohmic resistance, resistance corresponding to the high-frequency semicircle and reaction resistance respectively. Q_1 and Q_{dl} refer to constant phase elements corresponding to capacitance of the high-frequency semicircle and double-layer capacitance, respectively.

Equation (10) is rewritten as,

$$h = (\ln i_0 - \ln i)/a f. \quad (12)$$

By differentiating with respect to i, we obtain,

$$(dh/di)_{h\neq 0} = R_{ct} = -1/iaf. \quad (13)$$

By substituting for i from (10), we get

$$R_{ct} = e^{afh}/afi_0, \quad (14)$$

or, $$\ln R_{ct} + \ln(afi_0) = afh. \quad (15)$$

A plot of $\ln R_{ct}$ against h thus results in a straight line with a slope of (af) and an intercept of $\ln(afi_0)^{-1}$. It is thus possible to evaluate the values of a and i_0 from the impedance spectra of $Zr_{0.5}Ti_{0.5}V_{0.6}Cr_{0.2}Ni_{1.2}$ alloy electrode recorded at several potentials in HER regime. The variation in resistance R_{ct} of HER as a function of potential is shown in figure 9. The i_0 and a values derived are $5{\cdot}9 \times 10^{-4}$ A cm^{-2} and 0·343 respectively, which are nearly similar to those obtained from the Tafel polarization experiments (table 2).

An examination of the impedance parameters listed in table 3 suggests that the ohmic resistance (R_Ω) is nearly invariant in the range 1·1–1·6 Ù with overpotential. The magnitude of R_1 is small and it does not vary with overpotential in a systematic manner. A similar non-variance of this parameter is reported in the literature for HER at nickel electrodes (Chen and Lasia 1992; Dumont *et al* 1993). The value of n_1 corresponding to the Q_1 is close to unity, thus reflecting capacitive behaviour of this constant phase element. On the other hand, the value of n_2 (corresponding to Q_{dl}) is ~ 0·7, which deviates substantially from unity. Therefore, the constant phase element Q_{dl} could not be equated to C_{dl} of the electrode.

4. Conclusions

The study suggests that $Zr_{0.5}Ti_{0.5}V_{0.6}Cr_{0.2}Ni_{1.2}$ alloy ingot has the tendency to undergo corrosion in alkaline medium prior to its activation. But subsequent to the hydride formation, the corrosion of the alloy ingot is suppressed substantially which in turn helps to retain its hydrogen-storage capacity. The alloy is investigated for its corrosion resistance and hydrogen-evolution reaction (HER) in KOH electrolyte of varying concentrations. Prior to activation, the alloy electrode undergoes corrosion with oxygen-reduction reaction as a conjugate reaction. The corrosion-current density measured from Tafel polarization of (ORR) does not depend on KOH concentration. Alternating-current impedance spectra of the alloy electrode suggests capacitive behaviour of the electrode/electrolyte interface and the values of double-layer capacitance are in the range of 3–9 mF cm^{-2}. Subsequent to activation, the open-circuit potential of the electrode is shifted to the reversible potential of HER. The exchange current density values measured from Tafel polarization of HER are marginally higher in relation to the values obtained before the electrode is activated. Alternating current impedance spectra in the Nyquist form contain two overlapped semicircles. The high-frequency semicircle is attributed to the electrode geometry, whereas the low-frequency semicircle is due to the charge-transfer reaction and double-layer capacitance. The impedance data are analyzed by a non-linear least-square curve-fitting technique and impedance parameters are evaluated.

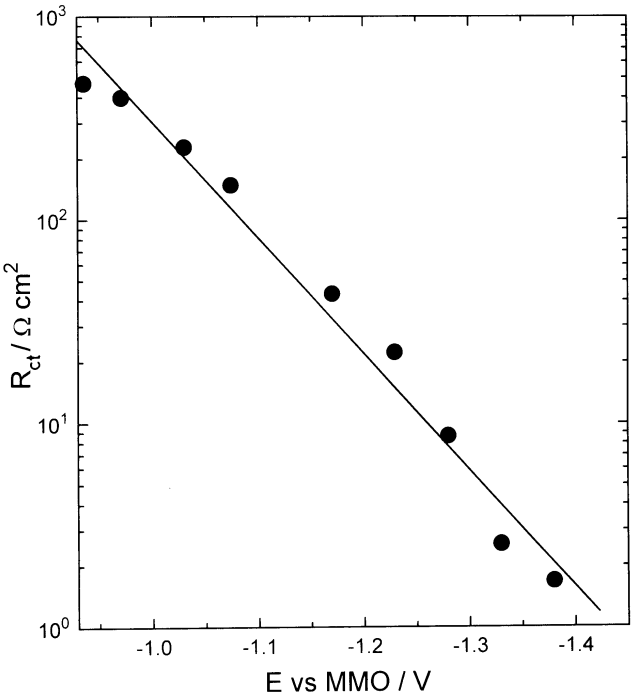

Figure 9. Variation of charge-transfer resistance (R_{ct}) of HER as a function of electrode potential (E).

References

Appleby A J, Kita H, Chemla M and Bronoel G 1973 *Encyclopedia of electrochemistry of the elements* (ed.) A J Bard (New York: Marcel Dekker, Inc) **Vol. 9**, p. 384

Boukamp B A 1989 *Equivalent circuit, Users manual* (The Netherlands: University of Twente)

Chen L and Lasia A 1991 *J. Electrochem. Soc.* **138** 3321

Chen L and Lasia A 1992 *J. Electrochem. Soc.* **139** 1058

Dumont H, Los P, Lasia A, Menard H and Brossard L 1993 *J. Appl. Electrochem.* **23** 684

Elumalai P, Vasan H N and Munichandraiah N 1999 *J. Solid State Electrochem.* **3** 470

Enyo M 1983 *Comprehensive treatise of electrochemistry* (eds) B E Conway, O'M Bockris, E Yeager, S U M Khan and R E White (New York: Plenum Press) **Vol. 7**, p. 241

Frumkin A N 1963 *Advances in electrochemistry and electrochemical engineering* (eds) P Delahay and C Tobais (New York: John Wiley & Sons) **Vol. 3**, p. 287

Ganesh Kumar V 1999 *Studies on nickel/metal–hydride, lithium–ion and valve regulated lead/acid batteries*, Ph.D. Thesis, Indian Institute of Science, Bangalore

Ganesh Kumar V, Shaju K M, Munichandraiah N and Shukla A K 1998 *J. Power Sources* **76** 106

Ganesh Kumar V, Shaju K M, Munichandraiah N and Shukla A K 1999 *J. Solid State Electrochem.* **3** 470

Ganesh Kumar V, Shaju K M, Rodrigues S, Munichandraiah N and Shukla A K 2000 *J. Appl. Electrochem.* **30** 349

Munichandraiah N, Scanlon L G and Marsh R A 1998 *J. Power Sources* **72** 203

Notoya R 1997 *Electrochim. Acta* **42** 899

Rodrigues S, Munichandraiah N and Shukla A K 1999a *J. Appl. Electrochem.* **29** 1285

Rodrigues S, Munichandraiah N and Shukla A K 1999b *J. Solid State Electrochem.* **3** 397

Rodrigues S, Munichandraiah N and Shukla A K 2000 *J. Appl. Electrochem.* **30** 373

Spataru N, Lehelloca J -G and Durand R 1996 *J. Appl. Electrochem.* **26** 397

Trasatti S 1992 *Advances in electrochemical science and engineering* (eds) H Gerischer and C W Tobias (Weinheim & New York: VCH) **Vol. 2**, p. 1